reproduced by permission of the AAS

THE ASTROPHYSICAL JOURNAL, 588:842–851, 2003 May 10
© 2003. The American Astronomical Society. All rights reserved. Printed in U.S.A.

THREE-DIMENSIONAL SIMULATIONS OF THE CHEMICAL AND DYNAMICAL EVOLUTION OF THE GALACTIC BULGE

NAOHITO NAKASATO[1,2] AND KEN'ICHI NOMOTO[1]
Received 2001 October 25; accepted 2003 January 15

ABSTRACT

A three-dimensional, hydrodynamical, *N*-body model for the formation of the Galaxy is presented, with special attention paid to the formation of the bulge component. Since none of the previous numerical models for the Galaxy's formation have a proper treatment of the chemical evolution and/or sufficient spatial resolutions, we have constructed a detailed model of the chemical and dynamical evolution of the Galaxy using our GRAPE smoothed particle hydrodynamics (SPH) code. Our SPH code includes various physical processes related to the formation of stellar systems. Starting with cosmologically motivated initial conditions, we obtain a stellar system qualitatively similar to the Galaxy. Then we analyze the chemical and kinematic properties of the bulge stars in our model and find qualitative agreement with observational data. The early evolution of our model has revealed that most bulge stars form during the subgalactic merger (merger component of the bulge stars). Because of the strong starburst induced by the merger, the metallicity distribution function of such stars becomes as wide as observed. We find that another group of the bulge stars forms later in the inner region of the disk (nonmerger component of the bulge stars). Because of the difference in the formation epoch, the main source of iron for this group of stars is different from that for the merger component. Iron in the merger and nonmerger components comes mainly from Type II and Type Ia supernovae, respectively. Since a Type Ia supernova ejects ~10 times more iron than a Type II supernova, [Fe/H] of the nonmerger component tends to be higher than that of the merger component, which widens the metallicity distribution function. From these results, we suggest that the Galactic bulge consists of two chemically different components; one has formed quickly through the subgalactic clump merger in the proto-Galaxy, and the other has formed gradually in the inner disk.

Subject headings: Galaxy: bulge — Galaxy: formation — hydrodynamics — stars: formation

1. INTRODUCTION

The formation of bulges, which are the high-density central component of spiral galaxies, is a key process in the formation of spiral galaxies. There are several scenarios for the formation process of the bulges (see, e.g., Bouwens, Cayon, & Silk 1999). Such scenarios can be divided into the following categories: (1) a primordial collapse (see, e.g., Eggen, Lynden-Bell, & Sandage 1962), (2) merging of subclumps in a protogalactic cloud (see, e.g., Baugh, Cole, & Frenk 1996), and (3) a secular evolution of a stellar disk (see, e.g., Norman, Sellwood, & Hasan 1996). Previously, the surface brightness of the bulges has been recognized to have the $R^{1/4}$ profile as in elliptical galaxies, where R denotes the distance from the center (see, e.g., Whitford 1978; Rich 1988). However, recent observations have revealed the presence of a class of bulges that are well fitted by the exponential profile (see, e.g., Andredakis, Peletier, & Balcells 1995); i.e., there exist two classes of bulges according to the surface brightness. Each formation scenario has advantages and disadvantages for explaining the diversity of bulges (Wyse 1999).

For the formation of the Galactic bulge, Matteucci & Brocato (1990) and Matteucci, Romano, & Molaro (1999) have constructed one-zone chemical evolution models as follows: (1) They assumed that the Galactic bulge was formed by a single starburst. In their best-fit model, the formation timescale is ~0.1 Gyr. (2) One of the predictions of their calculations is that the element ratio, such as [O/Fe], remains high even for metal-rich stars ([Fe/H] > 0) because the formation timescale of the bulge is shorter than the lifetime of a Type Ia supernova progenitor. However, the chemical properties predicted by the one-zone model depend strongly on their *assumption* of the dynamics, i.e., the formation timescale of the bulge. To constrain the formation scenarios, we need to calculate the chemical and dynamical evolution together and compare the model predictions with both the chemical and kinematic properties of the bulge.

Here we present the first results of our three-dimensional Galactic bulge formation model. We model the formation of the Galaxy by means of a smoothed particle hydrodynamics (SPH) method (Lucy 1977; Gingold & Monaghan 1977) that incorporates a star formation algorithm and a self-consistent treatment of the chemical enrichment history of gas. The three-dimensional models for the formation of disk galaxies have been investigated by many authors (e.g., Katz 1992; Steinmetz & Müller 1995; Friedli & Benz 1995; Berczik 1999), and they have succeeded in many respects. We follow the method and models by the previous authors but use a much larger number of particles to study the detailed formation and evolution processes of the Galaxy (Nakasato 2000).

In cold dark matter cosmology, the early stage of the formation of galaxies involves the progressive merging of subgalactic clumps (see, e.g., Baugh et al. 1996). To properly model the dynamics of the merger history, we adopt the

[1] Department of Astronomy, School of Science, University of Tokyo, Bunkyo-ku, Tokyo 113-0033, Japan; nakasato@astron.s.u-tokyo.ac.jp, nomoto@astron.s.u-tokyo.ac.jp.
[2] Astronomisches Rechen-Institut, Universität Heidelberg, Moenchhofstrasse 12-14, Heidelberg D-69120, Germany.

three-dimensional SPH method. The chemodynamical approach by Samland, Hensler, & Theis (1997), which is a mesh-based and two-dimensional method, is not suitable for modeling the early merging history of the protogalaxy.

Our SPH code uses the GRAPE (Sugimoto et al. 1990) and Remote-GRAPE systems (Nakasato, Mori, & Nomoto 1997) to compute the gravitational interaction between particles (GRAPE-SPH code). The adoption of the Remote-GRAPE system doubles the performance of our code since we can make the SPH calculation and N-body summation in parallel (Nakasato et al. 1997). This enhancement of performance enables us to use 7 times more particles than Katz (1992), Steinmetz & Müller (1995), and Raiteri, Villata, & Navarro (1996) so that the spatial resolution of our model is almost 2 times higher than their models. As a result, we can investigate the early merging history in much more detail during the Galaxy formation. We note that other authors (e.g., Navarro & Steinmetz 2000; Sommer-Larsen & Dolgov 2001) have published comparable or even higher resolution SPH galaxy formation models than the present work; however, these authors have mainly concentrated on the kinematic properties of the models. In contrast, in the present work, we have paid attention to both the chemical and kinematic properties.

Our study is the first attempt to model the formation and chemical evolution of the Galactic bulge using the self-consistent three-dimensional SPH method. Using the chemical and dynamical SPH code, we simulate the evolution of the Galaxy starting from a plausible cosmological initial condition. The obtained model well reproduces the important chemical and kinematic properties of the Galaxy, such as the formation of the bulge, disk, and halo (as seen in Fig. 5). By analyzing the results of this model, we construct a plausible scenario for the Galactic bulge formation.

The plan for the present paper is as follows: In § 2, we briefly describe our SPH method. Section 3 describes the procedure to construct initial conditions. We present a summary of results obtained with our model in § 4. By analyzing the result of our Galaxy model, we describe the formation history of the bulge component in § 5 and compare the chemical and kinematic properties of the bulge with recent observational results. Finally, § 6 is devoted to conclusions.

2. THE METHOD

We adopt the SPH method to construct self-consistent, three-dimensional, dynamical and chemical models for the formation of stellar systems. The SPH method has been applied to many astrophysical problems. Because of its Lagrangian nature, it is suitable to systems that have large density contrasts, e.g., the formation of galaxies (see, e.g., Evrard 1988; Hernquist & Katz 1989; Katz 1992; Steinmetz & Müller 1994), the evolution of galaxies (see, e.g., Friedli & Benz 1995; Patsis & Athanassoula 2000), cosmological simulations (see, e.g., Navarro & White 1994; Yoshikawa, Jing, & Suto 2000), and a cloud-cloud collision (see, e.g., Lattanzio et al. 1985; Habe & Ohta 1992). Various codes have been developed to combine SPH and N-body systems. In these codes, gravitational forces are calculated with various methods such as direct summations, particle-particle/particle-mesh methods (see, e.g., Evrard 1988), tree methods (see, e.g., Hernquist & Katz 1989; Benz et al. 1990), and the method using the special purpose computer GRAPE (see, e.g., Umemura et al. 1993; Steinmetz 1996).

To simulate the formation of a stellar system from gas, we use our GRAPE-SPH code, using the Remote-GRAPE library (Nakasato et al. 1997). The SPH formulation that we use is the same as that used by Navarro & White (1993). We use a spatially variable smoothing length and integrate equations of motion with a second-order Runge-Kutta method, as described in Navarro & White (1993). To simulate the formation of stellar systems from gas, our GRAPE-SPH code includes various physical processes related to the formation of stellar systems, e.g., cooling, star formation, and feedback by stars, as follows.

2.1. *Cooling and Star Formation*

We adopt the metallicity-dependent cooling functions, which are computed with the MAPPINGS III package by R. S. Sutherland (MAPPINGS III is the successor to MAPPINGS II described in Sutherland & Dopita 1993) to solve the energy equation of gas particles (see Fig. 1 of Nakasato, Mori, & Nomoto 2000 for the cooling functions actually used).

For the star formation algorithm, we adopt the star formation recipe as used in the usual SPH codes (Katz 1992). Hereafter, "STAR" means star particle, which is not an individual star but an association of many stars. In this recipe, we convert a fraction of a gas particle into a STAR when four conditions are satisfied. The first three conditions are the *physical* conditions, expressed as

$$(\nabla \cdot \boldsymbol{v})_i < 0 , \tag{1}$$

$$t_{\rm cool} < t_d , \tag{2}$$

$$t_d < t_{\rm sound} , \tag{3}$$

where $t_{\rm cool}$, t_d, and $t_{\rm sound}$ are the cooling time, dynamical time, and sound crossing time of the gas particle, respectively (see Nakasato et al. 2000 for the detailed timescale definition).

During each star formation interval ($\delta t = 2$ Myr in the present work), we check whether the three conditions are satisfied for each gas particle. If the gas particle satisfies these three conditions, we then check the fourth *probability* condition. Assuming that the star formation process is a Poisson process (Katz 1992), we can write the probability for star formation within δt as

$$P = 1.0 - \exp(-\delta t / t_{\rm star\,form}) , \tag{4}$$

where $t_{\rm star\,form}$ is the local star formation timescale. In our SPH code, we define $t_{\rm star\,form} = t_d / C$, where C is a parameter to control our star formation recipe. If P is larger than a random number (0–1), we create a new STAR from a fraction of the gas particle (star formation occurs!). Introducing this *probability* condition, we can effectively control the threshold density for star formation by changing the parameter C. We compute P as a function of the density (ρ) for different values of C, as shown in Figure 1. Here we assume $\delta t = 2$ Myr. Note that the time step used in the time integration is always smaller than δt. From Figure 1, we can see effects of C as follows: larger (smaller) C means a lower (higher) threshold density.

To demonstrate the dependence on the star formation parameter C, we evolve a spherical region of $10^{12}\ M_\odot$, which consists of 10% gas and 90% dark matter, for various C. Initially, we set up the sphere in rigid rotation and outward

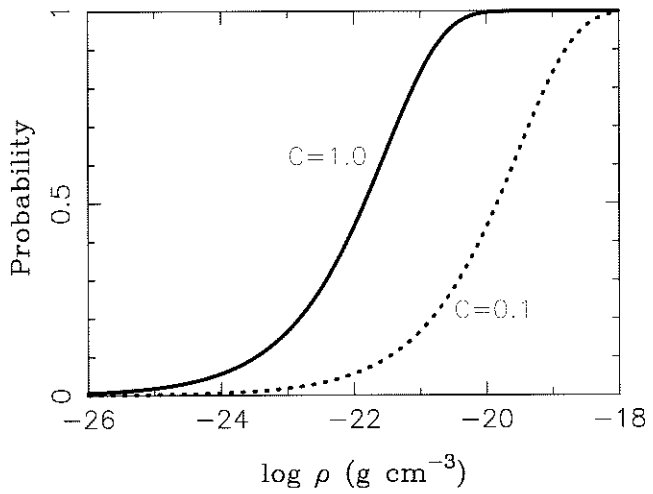

FIG. 1.—Star formation probability (P) as a function of gas density. The solid and dashed lines correspond to $C = 1.0$ and 0.1, respectively.

expansion, and the angular speed of rotation corresponds to the spin parameter $\lambda \sim 0.05$, where $\lambda = L|E|^{1/2}/GM^{5/2}$, with L being the angular momentum, E the total energy, M the mass, and G the gravitational constant (Padmanabhan 1993). This initial condition is the same as used in Katz (1992) and Steinmetz & Müller (1995). We evolve the sphere for three different star formation parameters, $C = 0.1$, 0.5, and 1.0. In Figure 2, we present the star formation history for $C = 0.1$ and 1.0. For $C = 1.0$, the star formation rates (SFRs) increase more rapidly than for $C = 0.1$ since the threshold density for star formation is lower. The STARs that formed early (i.e., very old STARs) in the $C = 1.0$ model have large vertical velocities. If we compare the projected edge-on surface density of STARs, the $C = 1.0$ model clearly shows more extended distribution than the $C = 0.1$ model. In Table 1, some kinematic properties at $t = 5$ Gyr are compared for different values of C. There is a clear correlation between C and the ratio between the X- and Z-axis velocity dispersions (or the spin parameter). From these results, we conclude that the $C = 0.1$ and 1.0 galaxies are

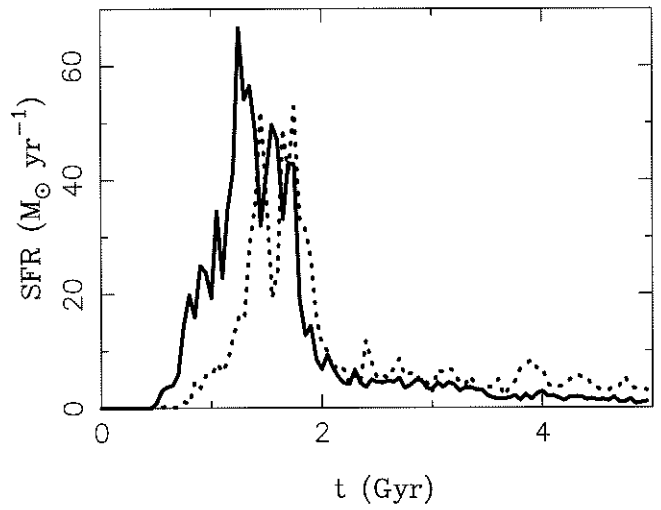

FIG. 2.—SFR as a function of time for galaxies with $C = 0.1$ (*dotted line*) and $C = 1.0$ (*solid line*).

TABLE 1

KINEMATIC PROPERTIES OF THE MODEL GALAXIES

C[a]	(σ_z/σ_x)[b]	Spin (λ)	Stellar Mass[c] ($\times 10^{10}\ M_\odot$)
0.1.....	0.59	0.70	4.2
0.5.....	0.71	0.52	5.4
1.0.....	0.77	0.44	4.6

[a] The star formation parameter.
[b] The ratio between the X- and Z-axis velocity dispersions.
[c] The stellar mass at $t = 5$ Gyr.

similar to late-type and early-type galaxies, respectively. To summarize, if we use this *probability* condition, various values of C lead to various global star formation histories. Hereafter, we set $C = 0.1$.

The mass of a newly formed STAR ($M_{\rm star}$) is calculated as

$$M_{\rm star} = \left[1 - \frac{1}{1 + 0.5(\delta t/t_{\rm star\,form})}\right] \pi h^3 \rho\ , \qquad (5)$$

where h and ρ are the smoothing length and the density of the gas particle, respectively (Nakasato et al. 2000). In the present calculation, the typical mass of STARs is $\sim 10^6$–$10^7\ M_\odot$.

2.2. *Feedback from Stars*

Formed stars eject energy and mass as stellar winds and supernova explosions (feedback from stars). As a result, stars heat up, accelerate, and enrich the circumstellar and interstellar medium. With current computing resources, it is not yet feasible to accurately include the energy, momentum, and mass feedback from stars in our SPH code. This is because the length resolution of the present calculation ($\sim$0.5 kpc) is much longer than the typical size of supernova remnants (<100 pc). Thus, in the present paper, we adopt a phenomenological method as adopted by several authors (e.g., Katz 1992) to mimic real feedback processes; i.e., we distribute the energy and mass ejected by a STAR to the neighboring gas particles. In our SPH code, we incorporate the effect of stellar winds and Type II and Type Ia supernova explosions as the energy and mass feedback processes. We compute the mass and energy ejection rates based on a simple model explained below. In this paper, we distribute the feedback energy as purely thermal energy. This treatment is a simple and zeroth-order approximation to the real nature, and other authors have tried to refine the treatment of feedback (e.g., Thacker & Couchman 2000; Springel & Hernquist 2002). Also in this paper, we follow the chemical evolution of total metal (Z), iron (Fe), and oxygen (O). The chemical evolution is coupled with the thermal and dynamical evolution; i.e., the ejected metal affects the evolution of gas through the metallicity-dependent cooling rates. To summarize, our GRAPE-SPH code is a most up-to-date SPH implementation for the formation of stellar systems and is used to successfully model the formation of globular clusters (Nakasato et al. 2000).

2.3. *Energy Ejection*

The energy ejection rate per STAR is given as

$$E_{\rm eject} = e_{\rm SW} R_{\rm SW} + e_{\rm SN\,II} R_{\rm SN\,II} + e_{\rm SN\,Ia} R_{\rm SN\,Ia}\ , \qquad (6)$$

where e_{SW} is the total energy ejected by stellar winds during the stellar lifetime and $e_{SN\,II}$ and $e_{SN\,Ia}$ are the energies ejected by Type II and Ia supernova explosions, respectively. The rate R_{SW} is the number of stars that expel their envelopes at the current epoch per unit time, and $R_{SN\,II}$ and $R_{SN\,Ia}$ are the rates of Type II and Type Ia supernovae, respectively. We define R_{SW} and $R_{SN\,II}$ as follows:

$$R_{SW} = \frac{\int_{M_{ms}}^{M_{up}} \phi(m)dm}{\tau(M_{ms})} , \quad (7)$$

$$R_{SN\,II} = \frac{\int_{M_{ms}}^{M_{ma}} \phi(m)dm}{\tau(M_{ms}) - \tau(M_{ma})} , \quad (8)$$

where $\phi(m)$ is the initial mass function (IMF), namely, $\phi(m)dm$ gives the number of stars in the mass range of $(m, m + dm)$, and $\tau(m)$ is the stellar lifetime as a function of stellar mass (David, Forman, & Jones 1990). In the present study, we assume the power-law–type IMF as

$$\phi(m) = Am^{-2.35} , \quad (9)$$

where A is a constant. For the upper and lower mass limits in the IMF, $M_{up} = 120\ M_\odot$ and $M_{lo} = 0.05\ M_\odot$ are assumed. In equations (7) and (8), M_{ma} (=50 $M_\odot$) and M_{ms} (=8 $M_\odot$) are the upper and lower mass limits of the stars that explode as Type II supernovae.

For the Type Ia supernova rate, we adopt the formulation given in the galactic chemical evolution model by Kobayashi et al. (1998) and Kobayashi, Tsujimoto, & Nomoto (2000). They adopt the single-degenerate scenario (Nomoto et al. 1994) for the Type Ia supernova progenitor, which is that a white dwarf (WD) in a close binary undergoes a thermonuclear explosion when the companion star evolves off the main sequence and transfers a large enough amount of mass to the WD. In their model, the Type Ia supernova rate at an epoch t is given as

$$R_{SN\,Ia}(t) = C_{SN\,Ia} \frac{\int_{M(t)}^{M(t+\Delta t)} \phi(m)dm}{\Delta t} , \quad (10)$$

where $M(t)$ is the mass of the companion star whose main-sequence lifetime is t and $C_{SN\,Ia}$ is a constant to be calibrated by the observational constraints. From the evolution model of the progenitor stars, Hachisu, Kato, & Nomoto (1996, 1999) obtained the mass ranges of the companion stars of the WDs that become Type Ia supernovae as

$$M_{sec} = [1.8,\ 2.6],\quad [0.9,\ 1.5]\ M_\odot . \quad (11)$$

We note that these mass ranges weakly depend on the metallicity of the star. In the present paper, we do not adopt the metallicity dependence. Figure 3 shows $R_{SN\,Ia}$ as a function of time, where we set $C_{SN\,Ia} = 1.0$. In the present paper, we set $C_{SN\,Ia} = 4.0 \times 10^{-4}$ from the result of test calculations. Note that other authors (Raiteri et al. 1996; Carraro, Lia, & Chiosi 1998) adopt different progenitor models by Greggio & Renzini (1983) and Matteucci & Greggio (1986).

For the supernova energy, we assume that $e_{SN\,II} = e_{SN\,Ia} = 10^{51}$ ergs. For the stellar wind energy, e_{SW} is estimated to be 0.2×10^{51} ergs for solar metallicity stars from the observational data of OB associations (Abbott 1982). The chemical abundance of a massive star significantly affects e_{SW} (Leitherer, Robert, & Drissen 1992), so that we use metallicity-dependent e_{SW} as $e_{SW} = 0.2e_{SN\,II}(Z/Z_\odot)^{0.8}$, where Z is the mass fraction of heavy elements in the STAR.

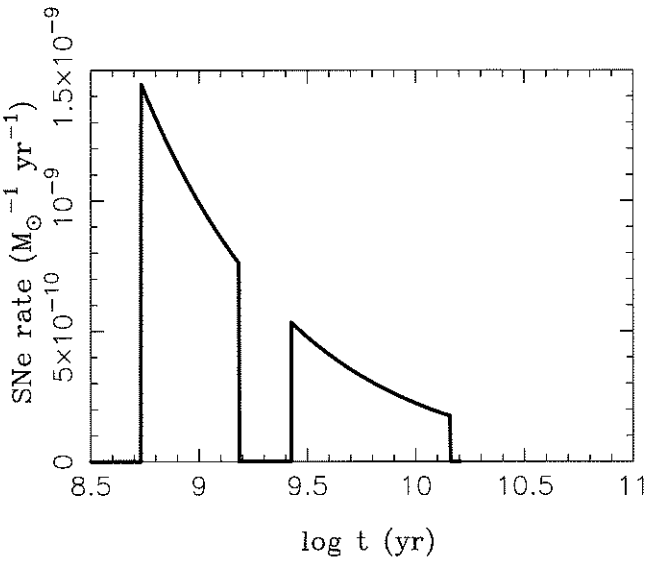

FIG. 3.—Type Ia supernova rate ($R_{SN\,Ia}$) as a function of time

2.4. *Mass Ejection*

In our code, the mass ejection in stellar winds from massive stars ($m \geq M_{ms}$) is combined with the mass ejection due to Type II supernovae. The mass ejection in stellar winds from low-mass stars ($m < M_{ms}$) is treated separately. Thus, the mass ejection rate per STAR is written as

$$M_{eject} = m_{SN\,II}R_{SN\,II} + m_{SWm}R_{SWm} + m_{SN\,Ia}R_{SN\,Ia} , \quad (12)$$

where $m_{SN\,II}$ is the average ejecta mass of Type II supernovae, m_{SWm} is the average mass ejected in stellar winds from the low-mass stars (corresponding to planetary nebulae), and $m_{SN\,Ia}$ is the ejecta mass of a Type Ia supernova. R_{SWm} is the number of stars per unit time expelling their envelopes at a certain epoch; $m_{SN\,II}$ and m_{SWm} are defined as

$$m_{SN\,II} = \frac{\int_{M_{ms}}^{M_{ma}} m\phi(m)dm}{\int_{M_{ms}}^{M_{ma}} \phi(m)dm} - m_{NS} , \quad (13)$$

$$m_{SWm} = \frac{\int_{M_{ll}}^{M_{ms}} m\phi(m)dm}{\int_{M_{ll}}^{M_{ms}} \phi(m)dm} - m_{WD} . \quad (14)$$

Here m_{NS} is the mass locked up in a neutron star and m_{WD} is the mass locked up in a WD. M_{ll} (=1 $M_\odot$) is the mass of the star whose lifetime nearly equals to the Hubble time. We set $m_{NS} = 1.4\ M_\odot$ and $m_{WD} = 1.4\ M_\odot$ and assume that a Type Ia supernova is produced by a Chandrasekhar-mass WD so that we set $m_{SN\,Ia} = 1.4\ M_\odot$. We define R_{SWm} as

$$R_{SWm} = \frac{\int_{M_{ll}}^{M_{ms}} \phi(m)dm}{\tau(M_{ll}) - \tau(M_{ms})} . \quad (15)$$

The fraction of heavy elements in $m_{SN\,II}$ and $m_{SN\,Ia}$ is computed using the nucleosynthesis yield of Type II and Ia supernovae (Tsujimoto et al. 1995; Nomoto et al. 1997). We compute the chemical evolution of total metal (Z), iron (Fe), and oxygen (O) in our code. The metallicity yield we used is tabulated in Table 2.

TABLE 2
HEAVY-ELEMENT YIELDS USED IN OUR CODE

SN Type	M^a ($M_\odot$)	Z ($M_\odot$)	Fe ($M_\odot$)	O ($M_\odot$)
Type II.....	14.0	2.54	0.091	1.80
Type Ia.....	1.4	1.4	0.74	0.14

NOTE.—These data are taken from Tsujimoto et al. 1995 and Nomoto et al. 1997.
[a] The total ejected mass per supernova explosion.

2.5. *Summary on Feedback*

The feedback phase is divided into three phases: a stellar wind phase, a Type II supernova phase, and a Type Ia supernova phase.

1. The stellar wind phase continues for $\tau(M_{\rm ma})$, during which only the energy ejection from STARs is included; the ejected mass is included in the Type II supernova phase for simplicity.
2. The Type II supernova phase begins at $t = \tau(M_{\rm ma})$ and ends at $t = \tau(M_{\rm ms})$. During this phase, the mass ejection rate is the sum of the contributions by stellar winds of massive stars and Type II supernovae.
3. The Type Ia supernova phase begins at $t = \tau(M_{\rm ms})$. During this phase, both the energy ejection and mass ejection rates are the sum of the contributions from Type Ia supernovae and stellar winds of low-mass stars.

We present the schematic view of the feedback processes in Figure 4.

With the present algorithm and the adopted parameters, a STAR of $10^8\ M_\odot$ produces $\sim 5.5 \times 10^5$ Type II supernova explosions and $\sim 1.4 \times 10^5$ Type Ia supernova explosions during 13 Gyr of the evolution. Also, $\sim 2.2 \times 10^7\ M_\odot$ of gas is ejected during the evolution. The ejected gas contains $\sim 1.6 \times 10^6\ M_\odot$ of heavy elements, which include $\sim 1.5 \times 10^5\ M_\odot$ of iron and $\sim 1.0 \times 10^6\ M_\odot$ of oxygen.

As a final note, the thermal energy, gas, and heavy elements from stellar winds and supernovae are smoothed over neighboring particles of the STAR within a neighboring radius of R_f (a feedback radius). R_f is a parameter set to 0.5 kpc, which is equal to the adopted gravitational softening length of STAR particles. Results of a test calculation with $R_f = 0.8$ kpc are very similar to those of the present paper.

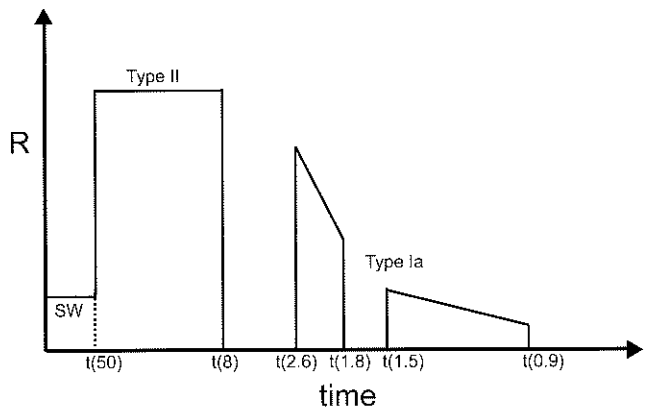

FIG. 4.—Schematic view of the feedback processes in our SPH code; "$t(m)$" is the stellar lifetime as a function of main-sequence mass ($m/M_\odot$).

3. INITIAL MODEL

Following previous work (e.g., Katz 1992), we investigate the evolution of the spherical 3 σ top-hat overdense region of a mixture of dark matter and gas with our SPH code. We neglect the matter outside the spherical regions, thus neglecting the late infall of the external matter and the external gravitational field. Throughout the paper, we set the Hubble constant $H_0 = 50$ km s^{-1} Mpc^{-1}, $\Omega = 1$, and $\Lambda = 0$. We set the initial redshift (z) of the model to be ~ 25 and the initial radius of the sphere to be 55 kpc. Thus, the comoving radius of the spherical region is ~ 1.4 Mpc and the contained mass is $\sim 10^{12}\ M_\odot$. We set the region in rigid rotation to provide a sufficient angular momentum with the spin parameter $\lambda \sim 0.1$. We also add the corresponding Hubble velocity to the velocity field of the sphere since we integrate the model with the physical coordinate.

To generate a 3 σ overdense region, we use the path integral method (Bertschinger 1987). We note that there are two further methods to set up the overdense region: (1) to seek the desired overdense region by sampling different random field realizations, which is used by the cosmological hydrodynamical simulations of formation of X-ray clusters (Anninos & Norman 1996) and (2) to select the desired halo from the results of the large-scale cosmological N-body simulations and use it as an initial condition for a cosmological galaxy formation model (Navarro & White 1994). The path integral method is the fastest method, and it is the easiest way to generate several dozen desired overdense regions, i.e., the overdense region of $10^{12}\ M_\odot$ in the present study. The weakness of this method is that we have to use the isolated boundary condition. Namely, we neglect the external tidal field and artificially add the angular momentum to the initial velocity field. On the other hand, with method 2, it is natural to use the surrounding particles as the origin of external tidal field. However, with method 2, it is difficult to find several overdense regions with similar properties since each region is very different, as in the real universe. We think that our way to generate initial conditions is an efficient way for our purpose of constructing the model for our Galaxy.

Specifically, initial models are constructed as follows: (1) We generate a spherical top-hat 3 σ overdense region with the path integral method (Bertschinger 1987). We use the COSMICS package[3] and generate 50 realizations. (2) We follow the nonlinear evolution of the dark matter particles in each spherical region with the same code. Note that we only use the N-body part of our GRAPE-SPH code in these simulations. (3) At a certain epoch ($z \sim 2.5$), we examine the properties of dark matter halos and select an appropriate realization for the hydrodynamical model. We select the model with a single halo since if two dominant halos exist, the gas disk will be destroyed by a major merger event (Barnes & Hernquist 1992). Among 50 realizations, 39 are single-halo models, and others are multiple-halo models. From 39 realizations, we select candidates for the hydrodynamical model by comparing the model density profile with the density profile of the Galactic halo. (4) Once we select several models, we restart the hydrodynamical N-body simulation from $z \sim 25$ with our GRAPE-SPH code. After we have done full hydrodynamical calculations for three single-halo models (and two multiple-halo models), we select the best-fit model, which is presented in this paper, by compar-

[3] See Bertschinger (1995) at http://arcturus.mit.edu/cosmics.

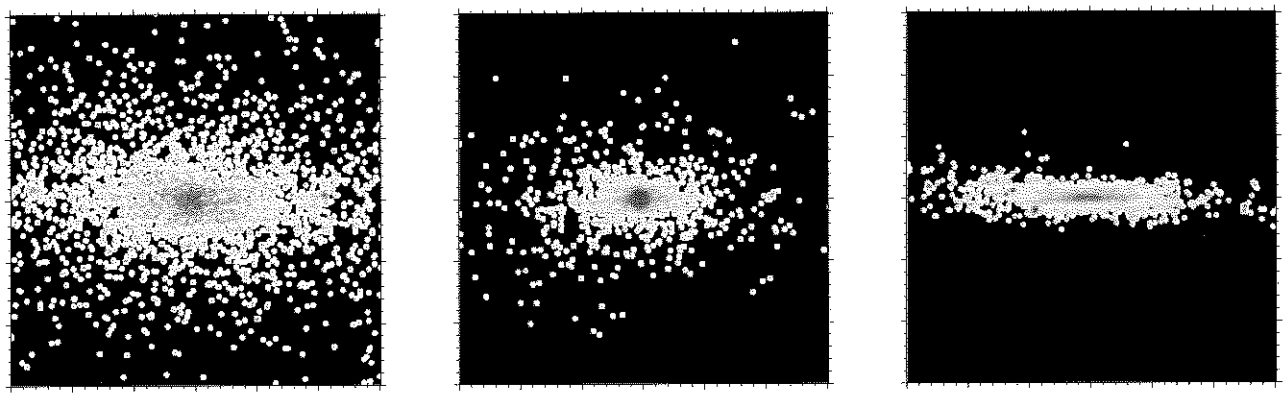

FIG. 5.—Projected STAR positions at $t = 5$ Gyr ($z \sim 1$) for the three components. From left to right, the metal-poor STARs, the metal-rich and old STARs, and the young STARs are shown (see text). The size of the panels is 20×20 kpc.

ing the disk scale length with the Galactic scale length. All results shown in the following sections are obtained with this best-fit model.

We have computed similar kind of models with several different configurations and found that the performance mainly depends on the speed of the GRAPE system: (1) For our old configuration using four GRAPE-3A boards, a similar calculation to the present work takes more than 200 hr up to $z \sim 0.9$ ($t = 5$ Gyr). (2) For our recent configuration using one GRAPE-5 board, a similar calculation takes only ~150 hr up to $z = 0$ ($t = 13$ Gyr). Using this recent configuration, a full hydrodynamical N-body computation for several dozen realizations is underway, and results will be presented elsewhere.

4. FORMATION OF THE GALAXY

The initial number of gas particles and dark matter particles is ~27,000 and ~27,000, respectively. Thus, with the total mass of $10^{12}\ M_\odot$, the initial masses of the gas particles and dark matter particles are 4×10^6 and $3.6 \times 10^7\ M_\odot$, respectively. We set the gravitational softening length for the gas and dark matter particles to be 0.5 and 1.0 kpc, respectively. The overall evolution is very similar to that in previously reported work (Steinmetz & Müller 1995; Berczik 1999). During the expansion due to the Hubble flow, small-scale structures grow and dense regions collapse. In such high-density regions (clumps), star formation occurs as a result of the efficient radiative cooling. These small clumps gradually merge to produce larger clumps. At $t \sim 0.3$–0.5 Gyr, these clumps merge, and the resulting clump becomes the primary halo that eventually becomes a spiral galaxy. Around this time ($z \sim 7$), the SFR reaches a maximum value. At $t \sim 1$ Gyr ($z \sim 4$), the dark matter is almost virialized, and the evolution of dark matter particles becomes a quasi-static state, while the gas particles are being settled into a thin disk. Finally, the prominent gas disk forms in the center of the primary halo at $t \sim 3$ Gyr ($z \sim 1.6$). Afterward, most star formation occurs in this gas disk, and the overall evolution becomes a quasi-static state.

After 5 Gyr of evolution (up to $z \sim 0.9$), over 80,000 STARs have formed, and the number of gas particles has decreased to ~13,000. At this stage, we categorize STARs according to the chemical properties and their formation epoch ($t_{\rm form}$), following the observational characteristics of the three components of the Galaxy as defined in Mihalas & Binney (1981).

Specifically, we categorize STARs by the following conditions and show the projected stellar densities in Figure 5:

1. *Left-hand panel.*—Metal-poor [$\log(Z/Z_\odot) < -3$] STARs.
2. *Middle panel.*—Old [$t_{\rm form} < 1$ Gyr] and metal-rich ($\log(Z/Z_\odot) > 0$) STARs.
3. *Right-hand panel.*—Young ($t_{\rm form} > 4$ Gyr) STARs.

Here Z is the mass fraction of heavy elements in STARs. Metal-poor STARs show an extended distribution since these STARs formed at an early epoch and at high latitude (*left*). The old and metal-rich STARs are concentrated in the galactic center (*middle*). The qualitative properties of the system are not so changed after $z \sim 1$ as reported by Steinmetz & Müller (1995). Since we neglect the late infall of surrounding material, the most recent star formation mainly occurs in the disk. As a result, the young STARs are located near the galactic plane (*right*). These results show that the calculated stellar system looks very similar to the Galaxy. To be more qualitative, we plot the face-on surface density profile of STARs in Figure 6. The crosses show our result. We fit the model with the following function: $\rho(r) = \rho_{\rm disk} \exp(-r/R_{\rm disk}) + \rho_{\rm bulge} \exp\{-7.67[(r/R_{\rm bulge})^{0.25} - 1]\}$, where

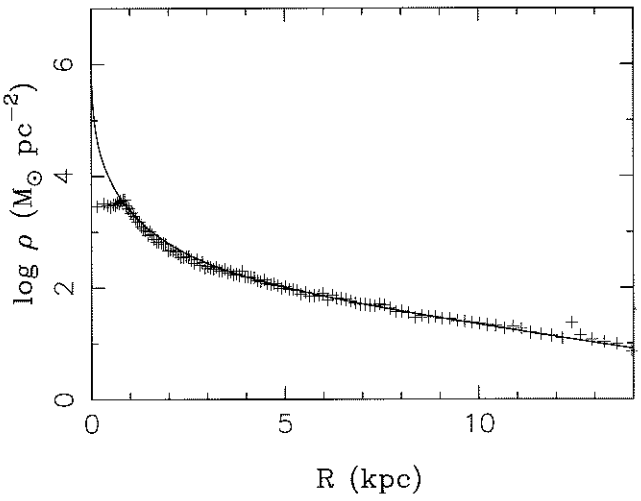

FIG. 6.—Face-on surface density of STARs at $t = 5$ Gyr. The crosses represent our model, and the solid line shows the fit to our model (see text).

the scale radii are $R_{\rm disk} = 4.21$ kpc and $R_{\rm bulge} = 0.876$ kpc. In the next section, we analyze the properties of STARs near the galactic center.

At $z = 0$, the total number of particles has increased to ~150,000, where the numbers of gas, dark matter, and STAR particles are ~11,000, 27,000, and 112,000, respectively. When we compare the projected density profile at $z \sim 0.9$ (Fig. 5) and $z = 0$, the three-component structure looks very similar except for the thickness of the disk STARs. Most star formation occurs quasi-statically near the disk plane, and the SFR is ~1–2 $M_\odot$ yr^{-1}.

5. FORMATION HISTORY OF THE BULGE COMPONENT

The one-zone chemical evolution model (see, e.g., Matteucci et al. 1999) predicted the approximate chemical properties of the Galactic bulge. To construct a self-consistent model of the bulge formation, however, a chemical and dynamical model is required. In this section, we use our high-resolution model for the formation and evolution of the galaxy to study the formation of the Galactic bulge.

5.1. *Dynamical History and Kinematics of the Bulge Stars*

We select the STARs located near the galactic center ($R < 2$ kpc) and define these STARs as the bulge stars. We define the center of the gravity of all STARs as the galactic center. To find the galactic center, we need several iterations to compute the center of the gravity. In the ith iteration, we compute the center of the gravity of STARs that are located within R_i kpc from the origin of the coordinate and convert the origin with that point. We set $R_1 = 20$ kpc and $R_2, R_3, \ldots = 5$ kpc. Typically, we only need three or four iterations. For example, at $z \sim 0.9$, the mass and number of bulge stars are $1.8 \times 10^{10}\ M_\odot$ and 16,800, respectively. After this time, we can select the bulge stars with the same definition. In this paper, however, we compare our model results at this time with some observational data. The reason is that in SPH models, including star formation recipes, the resolution of the model becomes worse and worse during the evolution since the number of gas particles decreases. With our chemical enrichment model, we need to have a large enough number of gas particles around a STAR particle to properly model the chemical evolution of the interstellar matter; further, the gas particles show a more extended distribution than the star particles, and this distribution makes the effective resolution of the chemical enrichment description worse. At $z \sim 0.9$, the number of gas particles becomes ~13,300, which is half of the initial number of gas particles and sufficiently large.

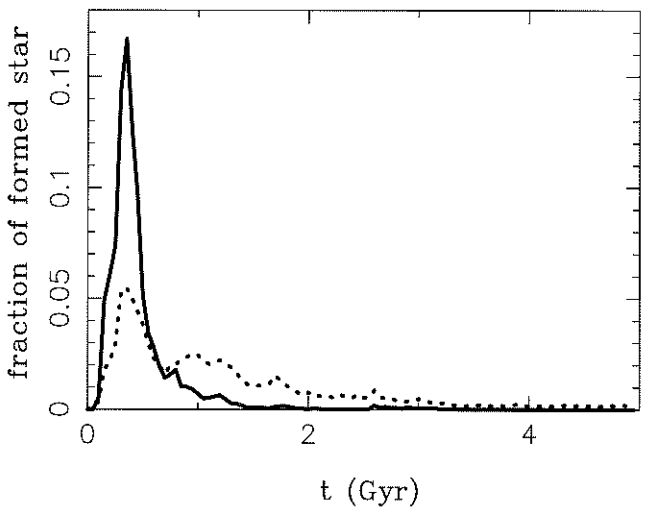

FIG. 7.—Star formation history for the bulge stars (*solid line*) and all stars (*dotted line*). The SFR divided by the total stellar mass of each population is shown as a function of time.

Figure 7 shows the SFR as a function of time for the bulge stars (*solid line*) and all stars (*dotted line*) up to $z \sim 0.9$. In this figure, we normalize the SFR by the total mass of each component at $z \sim 0.9$. More than 60% of the bulge stars up to this time formed during the first 0.5 Gyr of the evolution. With our model, we can obtain the detailed formation history of the bulge stars. In Figure 8, we present snapshots for projected STAR positions in the region where star formation is most violent for the first 0.5 Gyr. We note that the merging of two subgalactic clumps occurs during $t = 0.4$–0.5 Gyr. This merging of the clumps causes the starburst of the short timescale shown in Figure 7. Such a phenomenon is different from the simple starburst assumed in the one-zone chemical evolution model (Matteucci & Brocato 1990).

With our chemical and dynamical model, we can also obtain the kinematics of the bulge stars. In Figure 9, we plot the mean velocity (*upper line*) and the velocity dispersion (*lower line*) of these bulge stars. The bulge stars are substantially rotationally supported, with rotational speeds of ~160–230 km s^{-1}. These speeds are smaller than the rotational speeds of the disk stars (~270 km s^{-1} in the present

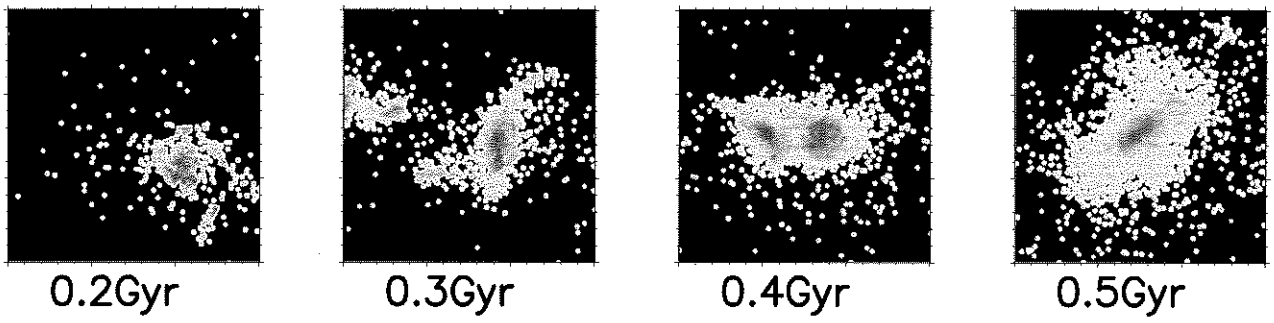

FIG. 8.—Projected STAR position for the first 0.5 Gyr of the evolution. During $t = 0.4$–0.5 Gyr, two clumps merge together. The size of the panels is 10×10 kpc.

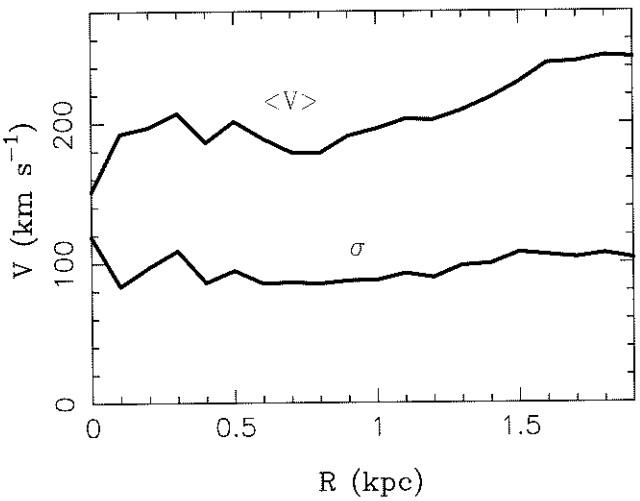

FIG. 9.—Mean velocity and the velocity dispersion for the bulge stars as a function of the distance from the galactic center. The upper and lower lines are the average velocity and the velocity dispersion, respectively.

model), which means that the angular momentum of the bulge is lost during the merging process. Figure 10 shows the x-direction velocity dispersion for the bulge stars as a function of [Fe/H]. Here our numerical results are shown by the filled triangles and filled squares and compared with observational data (Minniti 1996), shown by the dotted circles (note that the observational data are the line-of-sight velocity dispersion). The filled squares show the STARs with $t_{\rm form} < 1$ Gyr (old STARs), and the filled triangles show the STARs with $t_{\rm form} < 5$ Gyr (young STARs). The old and young STARs show a different trend, and the result for old STARs is more consistent with the observational data. Our model (especially old STARs) qualitatively reproduces the kinematic properties of the Galactic bulge.

5.2. *Chemical Properties of Bulge Stars*

The chemical properties of the bulge stars are important for constraining the formation of the Galactic bulge. In this subsection, we analyze the chemical properties of the bulge stars.

The observed metallicity distribution function of K giant stars (McWilliam & Rich 1994) is characterized by a wide ($-1.2 <$ [Fe/H] < 0.9) distribution, as shown by the dashed line in Figure 11. The distribution function of the bulge stars in our model (solid line in Fig. 11) is as wide as $-2.0 <$ [Fe/H] < 1.0, in good agreement with the observational data. As noted in the previous subsection, about 60% of the bulge stars form in the strong starburst caused by merging of subclumps (hereafter, these stars are called a merger component). This merger-driven starburst is partly responsible for this wide distribution. On the other hand, the other 40% of the bulge stars form in the late stage of evolution (a nonmerger component) and also contribute to widening the distribution function. This is because the nonmerger component of the bulge stars has much larger [Fe/H] than the merger component, as explained below.

The bulge stars can be divided into two chemically different types with and without being contaminated by Type Ia supernova ejecta. With the adopted progenitor model (Kobayashi et al. 1998), the epoch of the first appearance of Type Ia supernovae $t_{\rm SN\,Ia} = 0.5$ Gyr after the formation of each STAR. Thus, the STARs that formed after $t = 0.5$ Gyr are partially contaminated by Type Ia supernovae. Each Type Ia supernova ejects $\sim$10 times more iron than a Type II supernova (Nomoto et al. 1997). As a result, iron contained in the nonmerger component of the bulge stars partially originates from Type Ia supernovae, and their [Fe/H] tends to be higher than that of the merger component. In Figure 12, the distribution functions of the STARs that formed before and after $t = 0.5$ Gyr are plotted with the dashed and dotted lines, respectively, along with the total distribution function of the bulge stars (*solid line*). Both dashed and dotted lines show rather wide distributions, and clearly, the peak value of each distribution is different. The very old STARs, which form before $t = 0.5$ Gyr, contribute mainly to the metal-poor range of the distribution.

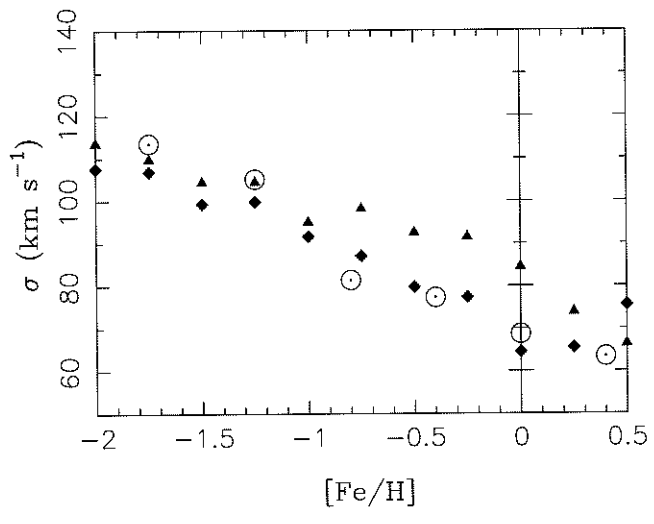

FIG. 10.—The x-direction velocity dispersion for the bulge stars as a function of [Fe/H]. The dotted circles show the observational data in Minniti (1996) (the error bound in the observation is $\sim$8–14 km s^{-1}). Our model STARs are shown by the filled squares ($t_{\rm form} < 1$ Gyr) and the filled triangles ($t_{\rm form} < 5$ Gyr).

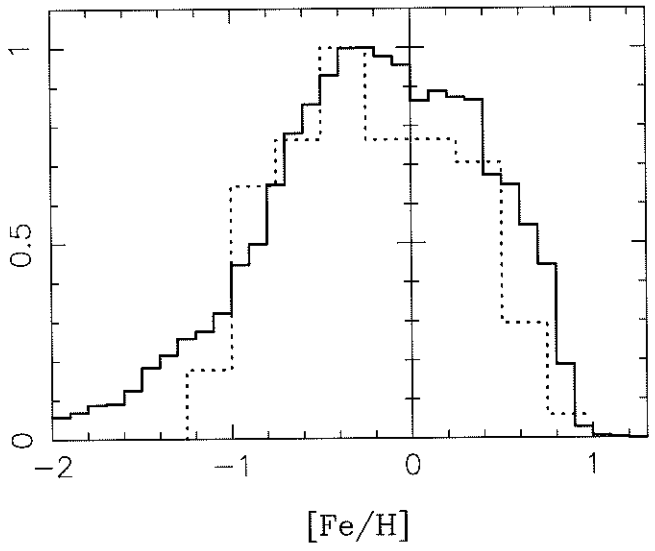

FIG. 11.—Calculated metallicity ([Fe/H]) distribution function of the bulge stars (*solid line*). The dashed line shows the observed metallicity distribution function of K giant stars (McWilliam & Rich 1994). The distributions are normalized by their maximum value for comparison.

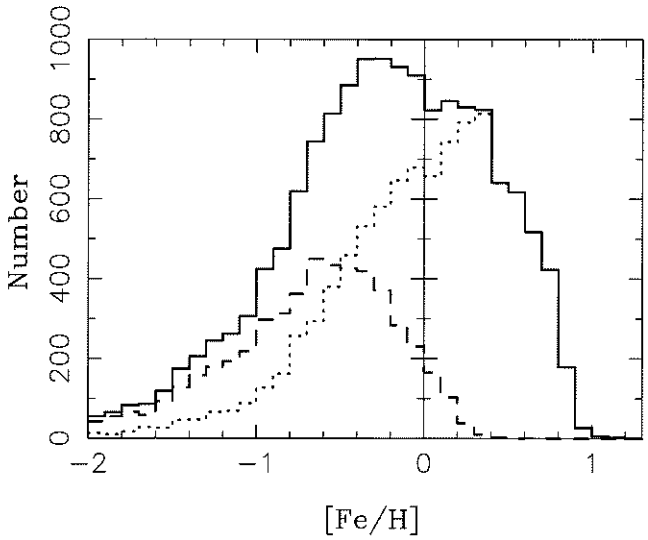

FIG. 12.—Calculated metallicity ([Fe/H]) distribution function of the bulge stars (*solid line*). The distributions are not normalized. The dashed and dotted lines correspond to the very old STARs with $t_{\rm form} < 0.5$ Gyr and young STARs with $t_{\rm form} \geq 0.5$ Gyr, respectively.

The adopted yields are [O/Fe] = 0.4 from Type II supernovae and [O/Fe] = −1.5 from Type Ia supernovae (Table 2). Thus, the contamination by Type Ia supernovae ejecta decreases [O/Fe] in STARs starting from [O/Fe] = 0.4. In Figure 13, we present the metallicity distribution function of the bulge stars for [O/Fe]. The very peaky distribution shows that half of the bulge stars have [O/Fe] ~ 0.4; i.e., half of the bulge stars are not contaminated by Type Ia supernovae. Also, almost 80% of the bulge stars have [O/Fe] > 0. Figure 14 shows [O/Fe] as a function of [Fe/H] for the bulge stars. [Fe/H] increases up to ~0.3 without Type Ia supernova contamination. Later, because of the increasing Fe enrichment by Type Ia supernovae, [O/Fe] decreases to roughly −0.4 as [Fe/H] increases to ~0.7. We note for a given [Fe/H] (>−0.5), [O/Fe] is distributed over a wide range of more than −0.4. Thus, even for [Fe/H] > 0, large fraction of the bulge stars have [O/Fe] > 0, while [O/Fe] is mostly subsolar for [Fe/H] > 0.3. These features of our model are consistent with the observed results as plotted in Figure 14 by the dotted circles (Rich & McWilliam 2000). The observed [Si/Fe] and [Ca/Fe] also show a relatively large dispersion from −0.4 to 0.2 for [Fe/H] > 0, although the observed results are still preliminary (Rich & McWilliam 2000).

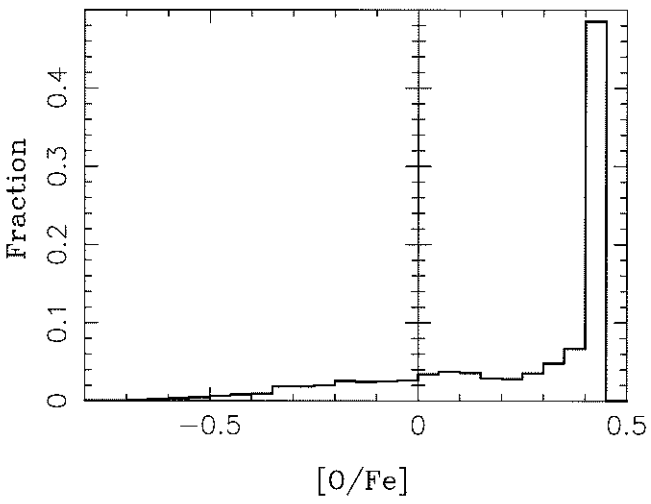

FIG. 13.—Calculated metallicity ([O/Fe]) distribution function of the bulge stars.

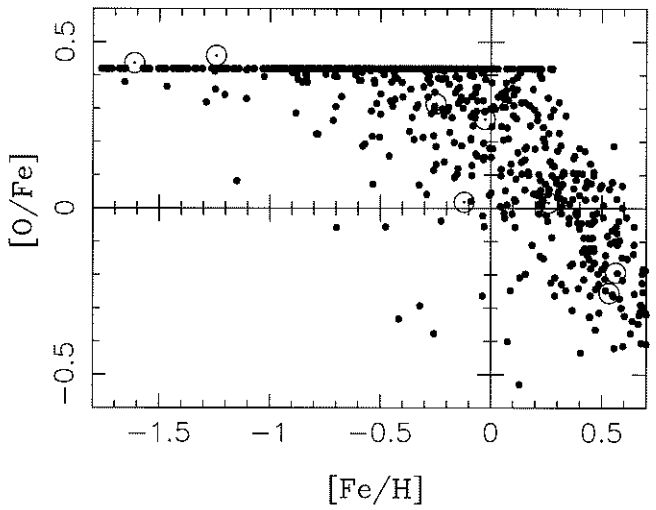

FIG. 14.—[O/Fe] vs. [Fe/H] for ~800 STARs, which are randomly selected from the bulge stars in our model (*filled circles*). The dotted circles show preliminary observational data (Rich & McWilliam 2000).

In contrast, Matteucci & Brocato (1990) argued that the metallicity of the bulge stars mainly originated from Type II supernovae. In their model, they assumed $t_{\rm SN\,Ia} \sim 1$ Gyr and that the star formation timescale is shorter than 1 Gyr, so that the majority of Type Ia supernovae have exploded long after the star formation. Therefore, the one-zone chemical evolution model predicts that the Galactic bulge is a chemically single population. In contrast to this picture, our chemical and dynamical model predicts that the Galactic bulge is neither a chemically single population nor a dynamically single population.

5.3. *Discussion*

There are several problems in our numerical model. First, the present model, which is compared with some observational data, is just the current best-fit model from only five realizations. Thus, the quantitative comparisons between our model and observations are still far from complete. One reason is that it is too difficult to find a consistent initial model for a very good match to the observations before doing real calculations. Because of complicated merging events occurring in the early phase, it is impossible to predict which initial halo will become a Milky Way–like spiral galaxy.

Another point is the resolution of the numerical model. As seen in Figure 6, the inner region of the present model is not well resolved. Thus, our definition radius for the bulge, $R < 2$ kpc, is not a clear definition when we compare our results with observational data. This is because Baade's window, where the chemical properties of the bulge stars are observed, is located 0.5 kpc from the galactic center. The choice of our definition is determined from the limitation of the numerical resolution of the present model. We use the rather large radius of 2 kpc to define the bulge stars since the gravitational softening length of the present model is 0.5 kpc (in fact, the inspection of Fig. 6 shows that the effective

resolution in our model is ~1 kpc, which equals the softening length of the dark matter particles). To summarize, the number of particles in the present model is still too small to fully resolve the chemical structure of the bulge. To make a more sensible comparison between numerical models and the observational data, we need much higher resolution models and more observational data obtained with large telescopes. Although there is such a limitation, our model is in good agreement with chemical and kinematic properties of the Galactic bulge stars.

6. CONCLUSION

In this paper, we report on the result of our high-resolution, three-dimensional models of the Galactic bulge formation. By modeling the formation and evolution of the Galaxy, we understand the formation history of the Galactic bulge as follows.

The early evolution of the best-fit model reveals that most bulge stars form during the merger that occurred in the region of the deepest potential. Because of the strong starburst induced by the merger, the metallicity distribution of the bulge component becomes as wide as observed. Although such a strong starburst has a similar effect as that of the burst assumed in the previous chemical evolution model, our model shows that there is another reason to widen the metallicity distribution function of the bulge. By analyzing our results, we find that the bulge stars in our model are composed of two different components. One component (merger component) was produced by the merger occurring in the center of the halo, as noted above. The other, nonmerger component was formed in the inner region of the disk after this merger. Because of the different formation epoch, the main source of iron for each component is different. Iron in the former comes mainly from Type II supernovae and in the latter from Type Ia supernovae. Since each Type Ia supernova ejects ~10 times more iron than a Type II supernova, [Fe/H] of the nonmerger component tends to be higher than that of the merger component, which widened the metallicity distribution function. Also, our model predicts a relatively large dispersion in [O/Fe] for [Fe/H] > 0.

Although our model is not in complete agreement with our Galaxy, some chemical and kinematic properties of the Galactic bulge, such as the velocity dispersion versus metallicity, are well reproduced. We thus conclude that an old fraction of the Galactic bulge is very likely to have been formed by the subclump merger in the protogalactic environment, while a younger fraction of the Galactic bulge has formed gradually in the inner disk. These two groups should show different chemical properties.

We would like to thank the anonymous referee for the valuable comments and suggestions to greatly improve the manuscript. Also, we would like to thank J. Makino for kindly providing access to the GRAPE-4 and GRAPE-5 systems, on which a part of the computation has been done. Some of the computation has been performed with the GRAPE cluster at the Astronomical Data Analysis Center of the National Astronomical Observatory, Japan. N. N. specially thanks the Astronomisches Rechen-Institut, Heidelberg, for the hospitality during the stay as a guest researcher when a part of the paper has been written. This work has been supported by JSPS Research Fellowships for Young Scientists (7664) and (05127), in part by an SFB 439 grant at the University of Heidelberg, and by grants-in-Aid for Scientific Research (07CE2002, 12640233, 14047206, 14540223) of Ministry of Education, Science, Culture, Sports, and Technology in Japan.

REFERENCES

Abbott, D. C. 1982, ApJ, 263, 723
Andredakis, Y. C., Peletier, R. F., & Balcells, M. 1995, MNRAS, 275, 874
Anninos, P., & Norman, M. 1996, ApJ, 459, 12
Barnes, J. E., & Hernquist, L. 1992, ARA&A, 30, 705
Baugh, C. M., Cole, S., & Frenk, C. S. 1996, MNRAS, 283, 1361
Benz, W., Bowers, R., Cameron, A., & Press, W. 1990, ApJ, 348, 647
Berczik, P. 1999, A&A, 348, 371
Bertschinger, E. 1987, ApJ, 323, L103
Bouwens, R., Cayon, L., & Silk, J. 1999, ApJ, 516, 77
Carraro, G., Lia, C., & Chiosi, C. 1998, MNRAS, 297, 1021
David, L. P., Forman, W., & Jones, C. 1990, ApJ, 359, 29
Eggen, O. J., Lynden-Bell, D., & Sandage, A. R. 1962, ApJ, 136, 748
Evrard, A. E. 1988, MNRAS, 235, 911
Friedli, D., & Benz, W. 1995, A&A, 301, 649
Gingold, A., & Monaghan, J. 1977, MNRAS, 181, 375
Greggio, L., & Renzini, A. 1983, A&A, 118, 217
Habe, A., & Ohta, K. 1992, PASJ, 44, 203
Hachisu, I., Kato, M., & Nomoto, K. 1996, ApJ, 470, L97
———. 1999, ApJ, 522, 487
Hernquist, L., & Katz, N. 1989, ApJS, 70, 419
Katz, N. 1992, ApJ, 391, 502
Kobayashi, C., Tsujimoto, T., & Nomoto, K. 2000, ApJ, 539, 26
Kobayashi, C., Tsujimoto, T., Nomoto, K., Hachisu, I., & Kato, M. 1998, ApJ, 503, L155
Lattanzio, C., Monaghan, J., Pongracic, H., & Schwarz, P. 1985, MNRAS, 215, 125
Leitherer, C., Robert, C., & Drissen, L. 1992, ApJ, 401, 596
Lucy, L. 1977, AJ, 82, 1013
Matteucci, F., & Brocato, E. 1990, ApJ, 365, 539
Matteucci, F., & Greggio, L. 1986, A&A, 154, 279
Matteucci, F., Romano, D., & Molaro, P. 1999, A&A, 341, 458
McWilliam, A., & Rich, R. M. 1994, ApJS, 91, 749
Mihalas, D., & Binney, J. 1981, Galactic Astronomy (2d ed.; New York: Freeman)
Minniti, D. 1996, ApJ, 459, 579
Nakasato, N. 2000, Ph.D. thesis, Univ. Tokyo
Nakasato, N., Mori, M., & Nomoto, K. 1997, ApJ, 484, 608
Nakasato, N., Mori, M., & Nomoto, K. 2000, ApJ, 535, 776
Navarro, J. F., & Steinmetz, M. 2000, ApJ, 538, 477
Navarro, J. F., & White, S. D. M. 1993, MNRAS, 265, 271
———. 1994, MNRAS, 267, 401
Nomoto, K., Hashimoto, M., Tsujimoto, T., Thielemann, F.-K., Kishimoto, N., Kubo, Y., & Nakasato, N. 1997, Nucl. Phys. A, 616, 79
Nomoto, K., Yamaoka, H., Shigeyama, T., Kumagai, S., & Tsujimoto, T. 1994, in Les Houches Session LIV, ed. S. A. Bludman (Amsterdam: Elsevier), 199
Norman, C. A., Sellwood, J. A., & Hasan, H. 1996, ApJ, 462, 114
Padmanabhan, T. 1993, Structure Formation in the Universe (Cambridge: Cambridge Univ. Press)
Patsis, P. A., & Athanassoula, E. 2000, A&A, 358, 45
Raiteri, C. M., Villata, M., & Navarro, J. F. 1996, A&A, 315, 105
Rich, R. M. 1988, AJ, 95, 828
Rich, R. M., & McWilliam, A. 2000, Proc. SPIE, 4005, 150
Samland, M., Hensler, G., & Theis, Ch. 1997, ApJ, 476, 544
Sommer-Larsen, J., & Dolgov, A. 2001, ApJ, 551, 608
Springel, V., & Hernquist, L. 2002, MNRAS, 333, 649
Steinmetz, M. 1996, MNRAS, 278, 1005
Steinmetz, M., & Müller, E. 1994, A&A, 281, L97
———. 1995, MNRAS, 276, 549
Sugimoto, D., Chikada, Y., Makino, J., Ito, T., Ebisuzaki, T., & Umemura, M. 1990, Nature, 345, 33
Sutherland, R. S., & Dopita, M. A. 1993, ApJS, 88, 253
Thacker, R. J., & Couchman, H. M. P. 2000, ApJ, 545, 728
Tsujimoto, T., Nomoto, K., Yoshii, Y., Hashimoto, M., Yanagida, S., & Thielemann, F.-K. 1995, MNRAS, 277, 945
Umemura, M., Fukushige, T., Makino, J., Ebisuzaki, T., Sugimoto, D., Turner, E., & Loeb, A. 1993, PASJ, 45, 311
Whitford, A. E. 1978, ApJ, 226, 777
Wyse, R. F. G. 1999, in The Formation of Galactic Bulges, ed. C. M. Carollo, H. C. Ferguson, & R. F. G. Wyse, R. F. G (Cambridge: Cambridge Univ. Press), 195
Yoshikawa, K., Jing, Y. P., & Suto, Y. 2000, ApJ, 535, 593